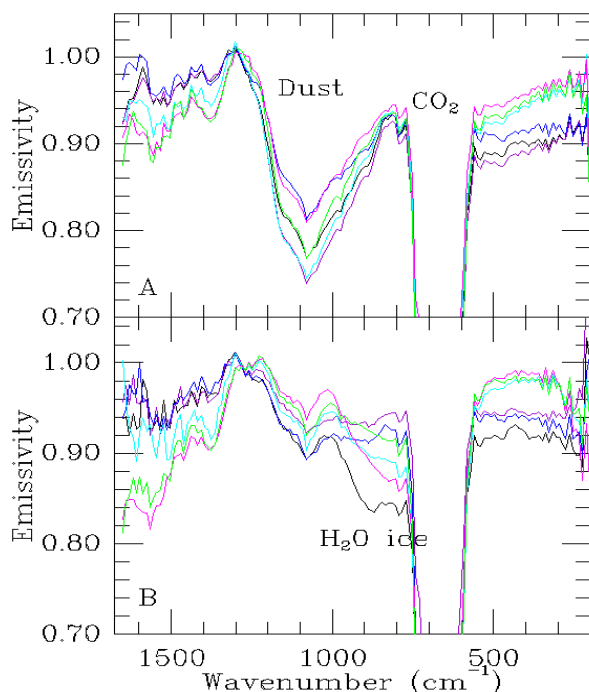


**THERMAL-INFRARED SPECTRAL CHARACTERISTICS OF MARTIAN ALBEDO FEATURES: CLUES TO COMPOSITION.** S. W. Ruff and P. R. Christensen, Arizona State University, Department of Geology, Tempe, AZ 85287-1404, ruff@tes.la.asu.edu.

**Introduction:** Thermal-infrared spectra of Mars are dominated by features attributable to atmospheric constituents. Dust, CO<sub>2</sub>, water vapor, and water ice all have strong absorptions in the thermal-infrared region that tend to obscure the spectral character of the surface and frustrate attempts to identify surface mineralogy. Any effort to examine Mars' surface spectral character must account for the atmosphere in some way. In the case of spectra measured by the Thermal Emission Spectrometer (TES), efforts are underway to account for atmospheric components using both radiative transfer analysis and a linear deconvolution strategy [1]. Both techniques are computationally intensive and are not readily available to users of TES data. However, empirical analysis of existing TES data has demonstrated that the bright and dark albedo features of Mars have unique spectral characteristics that are not obscured by the atmosphere. These characteristics persist across a range of atmospheric conditions and are mappable down to the smallest spatial resolution of TES data. Using carefully applied ratios of bright and dark region spectra, it is possible to cancel atmospheric spectral contributions to a degree that allows for compositional analysis of both bright and dark material on Mars' surface.

**Short and Long Wavelength Features:** The central region of TES spectra (~1300-600 cm<sup>-1</sup>) is dominated by an ever present CO<sub>2</sub> gas absorption and variable dust and water ice absorptions (Figure 1). Together, these features preclude the use of this spectral region for surface analysis when no atmospheric correction is used. Outside of this spectral region, atmospheric constituents are less dominant and surface spectral character is more readily discernable. This is most evident when comparing spectra from bright and dark regions on the planet. Figure 1 shows examples in which a few hundred spectra have been averaged together to create high signal-to-noise spectra of classic bright and dark regions of the planet. From these examples, spectral trends between bright and dark regions become apparent. At wavenumbers > 1300 (short wavelengths), bright regions have consistently lower emissivity than dark regions, evident even with CO<sub>2</sub> hot bands and water vapor features superimposed. The behavior at long wavelengths (< 600 cm<sup>-1</sup>) is reversed, with dark regions demonstrating lower emissivity than bright regions. Note that there is no apparent trend in the 1300-800 cm<sup>-1</sup> region where the variation of the atmospheric dust feature obscures any trend due to surface character.

These spectral trends persist even under differing atmospheric conditions. The examples shown in Figure 1a represent spectra from a period of high dust and



**Figure 1.** Average spectra of bright regions Isidis Planitia (cyan), Arabia Terra (magenta), and Amazonis Planitia (green), and dark regions Syrtis Major (black), Terra Tyrhena (purple), and Sinus Meridiani (blue). (A) Relatively high atmospheric dust and low water-ice opacity. (B) Low dust, higher water-ice opacity.

negligible water ice opacity. Figure 1b shows spectra from the same regions but during a period of lower dust and higher water-ice cloud opacity. Again, the same spectral behavior for bright and dark regions is evident. However, the absolute emissivity in both spectral regions has changed, precluding the use of absolute values to interpret non-atmospherically corrected spectra.

The thermal-infrared spectral behavior of bright and dark regions is evident at scales both regional (Figure 1) and local. Small-scale examples are best demonstrated by mapping the changes in long and/or short wavelengths using TES orbital tracks. Figure 2 shows how an average of 5 spectral channels at long wavelengths (530-480 cm<sup>-1</sup>) changes with albedo variations in the scene.

**Particle Size Effects:** It is possible to interpret the spectral behavior of bright and dark regions by combining concepts developed previously to understand Mars' albedo features with knowledge of laboratory spectra. It has long been accepted that dark regions on Mars represent coarse-particle (sand sized), dust-free surfaces and bright regions are fine-particle, dusty surfaces.

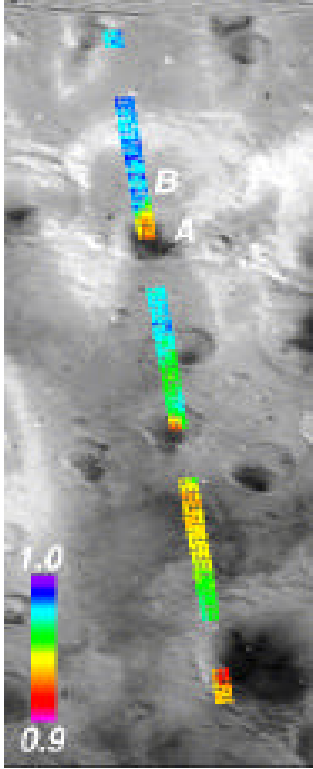


**Figure 2** Average emissivity from 530-480  $\text{cm}^{-1}$  for non-atmospherically corrected data (Eastern Xanthe Terra). A and B are described in text.

Because the thermal-infrared spectral behavior of minerals as well as rocks is particle size dependent, it is reasonable to expect that the spectra from these surfaces should display particle size effects. Silicates in particular display the generalized behavior of decreasing emissivity at short wavelengths and increasing emissivity at long wavelengths with decreasing particle size. These are the spectral trends in evidence in TES spectra of bright and dark regions. That is, the spectral behavior of Mars' albedo features is completely consistent with variation in particle size of silicate materials.

**Clues to Composition:** To go beyond the first order analysis of bright and dark regions and begin to address the question of composition, it is necessary to perform some form of atmospheric correction on the spectra. The relatively small spatial resolution of typical TES spectra (3 by 6 km pixels) means that ratios of closely spaced pixels can be used to cancel atmospheric contributions. The simplified equation that describes the total emittance reaching an orbiting sensor is

$$E_{\text{total}} = E_s * T_a + E_a \quad (1)$$

The emissivity of the surface ( $E_s$ ) is multiplied by the transmissivity of the atmosphere ( $T_a$ ) and added to the emissivity of atmospheric components. It is reasonable to assume that the constituents of a column of atmosphere are the same over two spots on the ground that are at the same elevation and close to one another.

Given this assumption, the value of  $T_a$  is the same over the chosen spots. Except during dust storms, atmospheric opacity is low and the  $E_a$  term is negligible. Therefore, a ratio of emissivity spectra from two proximal locations yields the equation

$$E_{\text{combined}} = E_{s_1} * T_a / E_{s_2} * T_a \quad (2)$$

In this treatment,  $T_a$  cancels leaving a ratio of the emissivity from the two surfaces. Intracratere dark material within a bright crater presents an ideal location to apply a spectral ratio (Figure 2, A and B). Because such a ratio contains spectral information from both dark and bright materials, it can not be compared directly with laboratory spectra. However, laboratory spectra that are themselves ratios of two spectra can be compared to TES spectral ratios. A surprisingly good match is obtained for ratios of dark to bright region spectra (Figure 2, A and B) using a ratio of laboratory spectra of coarse-particle pyroxene, plagioclase basalt (710-1000  $\mu\text{m}$ ) and its fine-particle equivalent (<63  $\mu\text{m}$ ) (Figure 3). The coarse- and fine-particle basalt spectra were chosen as possible examples of Martian dark and bright materials and have produced similarly good matches to other dark/bright ratios for many places on the planet. It remains to be determined how unique this solution is, but to date, spectral ratios using coarse- and fine-particle basaltic andesite and palagonite in varying combinations have failed to produce the same quality of fit. The work by [2] and [3] indicates a basaltic composition for Mars' dark regions similar to that used here. Therefore, the ratio technique produces results consistent with emerging information about Mars' dark materials but adds the intriguing possibility that bright regions may be simply ground up basaltic material.

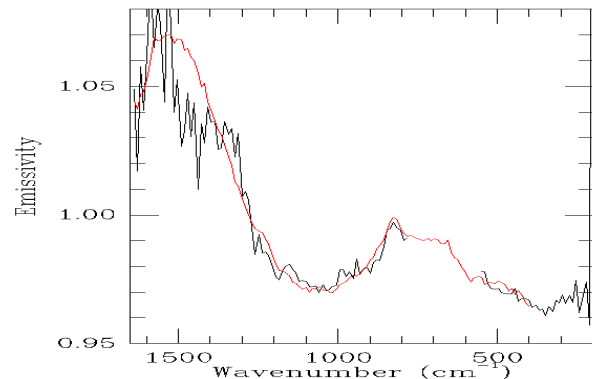


**Figure 3.** Ratio of A to B (black) from Fig. 2 compared with ratio of laboratory coarse- to fine-particle basalt (red).

**References:** [1] Smith, M. D. et al. (1999) *JGR* submitted. [2] Bandfield, J. L. et al. (1999) *LPSC XXX*. [3] Christensen, P. R. et al. (1999) *JGR* submitted.